

From Entanglement to Alignment: Representation Space Decomposition for Unsupervised Time Series Domain Adaptation

Rongyao Cai¹, Ming Jin², Qingsong Wen³, Kexin Zhang^{1*}

¹Institute of Cyber-Systems and Control, Zhejiang University, Hangzhou, China

²School of Information and Communication Technology, Griffith University, Brisbane, Australia

³Squirrel Ai Learning, Bellevue, USA

{rycai, zhangkexin}@zju.edu.cn, ming.jin@griffith.edu.au, qingsongedu@gmail.com

Abstract

Domain shift poses a fundamental challenge in time series analysis, where models trained on source domain often fail dramatically when applied in target domain with different yet similar distributions. While current unsupervised domain adaptation (UDA) methods attempt to align cross-domain feature distributions, they typically treat features as indivisible entities, ignoring their intrinsic compositions that govern domain adaptation. We introduce **DARSD**, a novel UDA framework with **theoretical explainability** that explicitly realizes UDA tasks from the perspective of **representation space decomposition**. Our core insight is that effective domain adaptation requires not just alignment, but principled disentanglement of transferable knowledge from mixed representations. DARSD consists of three synergistic components: **(I)** An adversarial learnable common invariant basis that projects original features into a domain-invariant subspace while preserving semantic content; **(II)** A prototypical pseudo-labeling mechanism that dynamically separates target features based on confidence, hindering error accumulation; **(III)** A hybrid contrastive optimization strategy that simultaneously enforces feature clustering and consistency while mitigating emerging distribution gaps. Comprehensive experiments conducted on four benchmarks (WISDM, HAR, HHAR, and MFD) demonstrate DARSD's superiority against 12 UDA algorithms, achieving optimal performance in 35 out of 53 scenarios and ranking first across all benchmarks.

Introduction

In the context of rapid development of time series analysis, domain adaptation has emerged as a critical bottleneck of practical algorithm deployment across diverse environments (Zhang et al. 2024a; Fang et al. 2024). Consider a human activity recognition system trained on smartphone accelerometer data from young adults in a lab, its accuracy can drop sharply when used on smartwatches worn by elderly users in daily life (Zhao et al. 2025). This dramatic performance degradation stems from a fundamental issue: while the underlying patterns of human activities stay the same, like walking still exhibits periodic acceleration patterns, the data distributions shift significantly due to fluctuations in objects, environments, or perception (Zhao et al. 2021). Such domain shift scenarios are widespread across

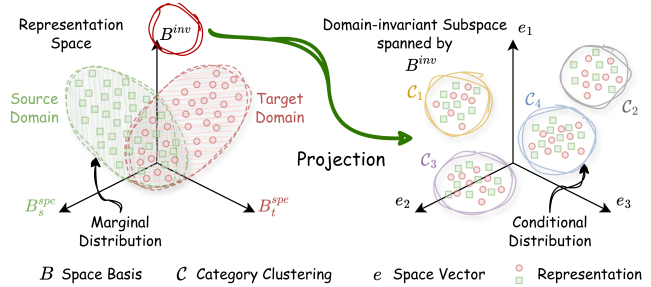


Figure 1: Visual description of representation space decomposition. We disentangle the basis of representation space into invariant one B^{inv} and specific ones related to domains B_s^{spe} and B_t^{spe} , aiming to achieve discriminative clustering in domain-invariant subspace spanned by B^{inv} .

real-world applications ranging from industrial equipment monitoring (Cai et al. 2024a; An et al. 2025) to healthcare sensing (Ye and Wang 2024).

Due to a lack of expert knowledge or high cost (Ozyurt, Feuerriegel, and Zhang 2023; Zhang et al. 2024b), the ground truth of target domain is not available during training in most scenarios. Unsupervised domain adaptation (UDA) has gained increasing attention, which trains a robust model using annotated source data with unlabeled target data, aiming to achieve good performance on the latter (Zhang et al. 2024a; Westfechtel et al. 2024). Notably, source and target domain exhibit similar yet distinct distributions.

Existing UDA approaches attempt to address domain shift through feature distribution alignment, they can be classified into three main categories. **Adversarial training methods** (Wang, Yang, and Yu 2024; Xie et al. 2025) learn domain-confusing representations by fooling discriminators (Lu et al. 2024). But this adversarial game often lacks supervision linked to downstream tasks, eliminating meaningful patterns alongside domain-specific artifacts. **Metric learning approaches** (Zhu et al. 2021; Zha et al. 2025) minimize statistical distances between source and target distributions (Lu et al. 2024), yet they impose an unrealistic assumption that entire features need be aligned, despite the fact that only part of components carry transferable knowledge. **Self-supervised methods** (Xu et al. 2025; He et al. 2023)

*Correspondence to: Kexin Zhang (zhangkexin@zju.edu.cn).

depend on contrastive learning with pretext tasks, such as pseudo-labeling (Chen et al. 2021). However, they run into a problem that label noise tends to build up progressively over the course of training. The core flaw underlying above approaches is that they treat features as **monolithic and indivisible entities**, implicitly hoping for invariance through distribution matching, overlooking the fact that effective domain adaptation demands *a principled distinction between what ought to transfer and what ought not to*. Though several methods have been proposed based on the insight of feature decomposition, they rely on the implicit network structure (Chen et al. 2024; Qu et al. 2024) or causal hidden variables (Lu and Sun 2024).

Our work is motivated by a key insight from representation learning: *features possess internal structure*, as depicted in Fig. 1. Domain shift primarily impacts certain dimensions of representations while leaving others unaltered. For instance, in accelerometer data, the temporal dynamics of walking remain largely consistent across devices (*domain-invariant*), whereas sensor noise characteristics and sampling artifacts vary significantly (*domain-specific*). This observation suggests a conceptual shift, *instead of aligning entire feature distributions, we should explicitly decouple representations into orthogonal subspaces and selectively transfer only the invariant components*. Such decomposition not only preserves semantic information but also provides interpretable insights into which patterns actually transfer across domains.

Based on this perspective, we introduce **DARSD** (**D**omain **A**daptation **v**ia **R**epresentation **S**pace **D**ecomposition), a novel UDA framework that explicitly disentangles domain-invariant from domain-specific feature components. To achieve this goal, DARSD employs three synergistic innovations: **(I) Adversarial Learnable Common Invariant Basis (Adv-LCIB)**: a learnable orthogonal transformation that projects source and target features into a shared domain-invariant subspace while adversarially remaining the information completeness; **(II) Prototypical Pseudo-label Generation with Confidence Evaluation (PPGCE)**: a dynamic mechanism that assigns reliable pseudo-labels to target features, partitions them by confidence, and thereby prevents the accumulation of label noise; **(III) Hybrid Contrastive Optimization**: a carefully designed collaborative optimization architecture that balances feature clustering for discrimination with consistency enforcement for robustness. Briefly put, our key contributions are summarized as follows:

- **Innovative Paradigm:** To the best of our knowledge, **DARSD** is the first explicit representation space decomposition framework for time series UDA tasks.
- **Interpretable Theory:** We propose a novel Adv-LCIB mechanism with theoretical foundations to conduct feature projection and domain-invariant pattern extraction.
- **Robust Optimization:** We introduce a hybrid contrastive optimization strategy integrated with the PPGCE module to implement differentiated treatment of cross-domain features, creating homogeneous yet discriminative category-wise feature distributions.

- **Experimental Evaluation:** Comprehensive experiments on four benchmarks against 12 UDA algorithms demonstrate the superior performance of our DARSD framework, achieving 35 out of 53 SOTA results.

Problem Definition

UDA for time series essentially boils down to a classification task involving samples from divergent distributions. Given an annotated source dataset \mathcal{S} and an unannotated target dataset \mathcal{T} , which follow similar yet different distributions, the objective of UDA is to predict the labels of \mathcal{T} . Specifically, \mathcal{S} is denoted as $\{(x_i^s, y_i^s)\}_{i=1}^{n_s} \sim \mathcal{D}_s$, comprising n_s samples drawn from distribution \mathcal{D}_s . Here, $x_i^s \in \mathbb{R}^{T \times D}$ represents a source sample capturing D sensors over T time points and each label y_i^s belongs to the label set \mathcal{C} with n_c categories. \mathcal{T} is defined as $\{(x_i^t)\}_{i=1}^{n_t} \sim \mathcal{D}_t$ with n_t samples following distribution \mathcal{D}_t , where $x_i^t \in \mathbb{R}^{T \times D}$ denotes a target sample with unknown label $y_i^t \in \mathcal{C}$.

Our objective is to train a robust feature extractor $FE(\cdot)$ by leveraging annotated \mathcal{S} and unlabeled \mathcal{T} . This extractor will derive a domain-invariant feature set $F = \{F_s \cup F_t\}_{n_s+n_t}^{n_s+n_t}$ from \mathcal{S} and \mathcal{T} . Subsequently, we fine-tune a classifier $CLF(\cdot)$ using $\{(f_i^s, y_i^s)\}_{i=1}^{n_s}$ to predict the label set $Y_t = \{y_i^t\}_{i=1}^{n_t}$ for \mathcal{T} based on the feature set $F_t = \{f_i^t\}_{i=1}^{n_t}$.

Methodology

The detailed pre-training procedure of our DARSD framework is illustrated in Fig. 2. DARSD comprises a shared feature extractor $FE(\cdot)$, an Adv-LCIB module, and a hybrid contrastive optimization mechanism integrated with the PPGCE module.

Adversarial Learnable Common Invariant Basis

The fundamental insight guiding our approach is that features are compositional that they can be decomposed into orthogonal components serving distinct functional roles. In time series data, specific feature dimensions capture semantic patterns consistent across domains (*e.g.*, temporal correlations, periodic structures, trend characteristics), whereas others encode domain-varying environmental artifacts (*e.g.*, sampling noise, device-specific biases, environmental interference). Traditional UDA methods seek to align entire feature distributions, which inadvertently mixes these heterogeneous components, compromising both semantic preservation and domain invariance.

Our key innovation lies in explicitly achieving decomposition via Adv-LCIB module. Rather than relying on implicit alignment to preserve semantic content, we construct an observed learnable orthogonal basis $B_{obs}^{inv} \in \mathbb{R}^{d \times m}$ that spans a domain-invariant subspace. This basis acts as a semantic filter, projecting features into a subspace that captures transferable patterns while excluding domain-specific artifacts.

Feature Decomposition Principle: Any feature $f \in \mathbb{R}^d$ regardless of domains can be conceptually decomposed as:

$$f = FE(x) = f^{inv} + f^{spe} \quad (1)$$

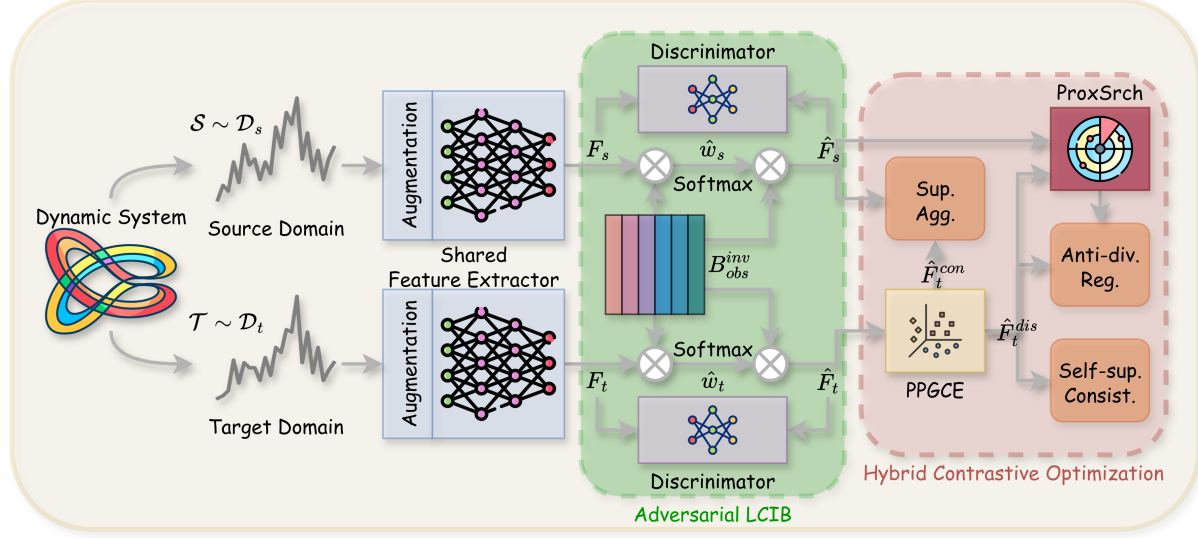


Figure 2: The DARSD framework for time series domain adaptation. Features are first projected into a domain-invariant subspace (Adv-LCIB), then target features receive pseudo-labels with confidence evaluation (PPGCE), and finally all features undergo hybrid contrastive optimization for category-wise aggregation across domains. In hybrid contrastive optimization block, (1) *Sup. Agg.*, (2) *Self-sup. Consist.*, (3) *Anti-div. Reg.*, and (4) *ProxSrch* are the abbreviations of (1) *Supervised Aggregation*, (2) *Self-supervised Consistency*, (3) *Anti-divergence Regularization*, and (4) *Proximity Searcher*, respectively.

where f^{inv} contains domain-invariant semantic patterns and f^{spe} contains domain-specific artifacts. Our goal is to extract f^{inv} without explicit prior knowledge of this decomposition.

Learnable Basis Construction: We introduce a learnable orthogonal matrix $B_{obs}^{inv} \in \mathbb{R}^{d \times m}$, spanning the domain-invariant subspace. For any given feature f , its domain-invariant representation is calculated as follows:

$$\begin{aligned} w^{inv} &= (B_{obs}^{inv})^\top f \\ &= (B_{obs}^{inv})^\top (f^{inv} + f^{spe}) \\ &= (B_{obs}^{inv})^\top f^{inv} = (B_{obs}^{inv})^\top B^{inv} w^{inv} \\ \hat{f} &= B_{obs}^{inv} w^{inv} \end{aligned} \quad (2)$$

where w^{inv} denotes the coordinate of f in domain-invariant subspace spanned by B^{inv} . B_{obs}^{inv} is the observed approximation of authentic invariant space basis B^{inv} . The **proof of Eq. (2)** is depicted in **Appendix B**.

During training process, B_{obs}^{inv} gradually approaches B^{inv} but may inadvertently incorporate some domain-specific artifacts. Given that invariant patterns dominate B_{obs}^{inv} while domain-specific artifacts account for a smaller proportion, DARSD employs the softmax regularization to amplify the weight differences between them. This operation suppresses domain-specific noise, thereby ensuring the efficiency of invariant information in the reconstructed features \hat{f} .

$$\hat{w} = \text{Softmax}(w^{inv}) = \text{Softmax}((B_{obs}^{inv})^\top FE(x)) \quad (4)$$

$$\hat{f} = B_{obs}^{inv} \hat{w} = B_{obs}^{inv} \text{Softmax}((B_{obs}^{inv})^\top FE(x)) \quad (5)$$

Overall, LCIB module consists of the following stages:

(1) Projection: B_{obs}^{inv} projects feature f onto the invariant

subspace to obtain the coordinate w^{inv} . **(2) Softmax Regularization:** Ensures only the most relevant invariant components are retained, naturally suppressing domain-specific noise and yielding \hat{w} . **(3) Reconstruction:** B_{obs}^{inv} reconstructs the domain-invariant representation \hat{f} using coordinate \hat{w} .

Adversarial Solution: LCIB is agnostic to the quality of B_{obs}^{inv} , whether it truly captures domain-invariant patterns or merely memorizes input features. A naive, unconstrained basis might inadvertently retain unintended domain-specific noise while missing out on expected domain-invariant patterns, defeating the purpose of decomposition.

To tackle this issue, we analyze the proportion of f^{inv} and f^{spe} within f . f^{spe} primarily captures distribution shifts induced by dynamic sampling environments, whereas f^{inv} encodes essential characteristics that remain consistent across domains. Given their critical role in domain adaptation, we hypothesize that f^{inv} should govern features f . To this end, DARSD incorporates a discriminator $D(\cdot) : \mathbb{R}^d \rightarrow [0, 1]$ tasked with distinguishing between original features f and corresponding reconstructed counterparts \hat{f} with the goal of keeping f^{inv} as much as possible. The discriminator is trained to maximize:

$$\mathcal{L}^{adv} = \mathbb{E}_{\bar{f}_i \in \{F \cup \hat{F}\}} \left[z_i \log(D(\bar{f}_i)) + (1 - z_i) \log(1 - D(\bar{f}_i)) \right] \quad (6)$$

where z_i is assigned label for $\bar{f}_i \in \{F \cup \hat{F}\}$.

Prototypical Pseudo-label Generation with Confidence Evaluation

The domain-invariant feature sets \hat{F}_s and \hat{F}_t derived from Adv-LCIB create an opportunity for effective cross-domain

knowledge transfer. However, a critical asymmetry persists: source features are accompanied by ground-truth labels, enabling supervised learning and category-wise clustering, while target features lack supervisory signals and thus cannot directly participate in discriminative optimization.

To fully leverage target features, assigning reliable pseudo-labels to \hat{F}_t is a viable solution, allowing them to join source features in supervised learning. This enables category-wise aggregation, where features from the same semantic class are clustered together regardless of domains, while those from different classes are separated. Even so, pseudo-labels vary in trustworthiness, that unreliable ones can introduce noise, degrade the quality of clustering, and disrupt decision boundaries. We need a mechanism to distinguish reliable from unreliable pseudo-labels and treat them differently during optimization.

Rather than relying on classifier predictions that may be biased toward source domain characteristics, we generate pseudo-labels through prototypical similarity in the domain-invariant subspace. This approach capitalizes on the geometric structure of reconstructed invariant representations.

Momentum-based Prototype Construction: For each class $c \in \mathcal{C}$, we maintain a prototype p_c that serves as the centroid of class c within the domain-invariant subspace:

$$p_c^{t+1} = \mu p_c^t + (1 - \mu) \frac{1}{|\mathcal{S}_c|} \sum_{\hat{f}_i^s \in \mathcal{S}_c} \hat{f}_i^s \quad (7)$$

where $\mathcal{S}_c = \{\hat{f}_i | y_i^s = c, \hat{f}_i \in \hat{F}_s\}$ contains source features of class c , and μ controls the momentum factor.

Pseudo-label Assignment: For each target feature \hat{f}_j^t , we assign pseudo-label based on maximum cosine similarity:

$$y_i^{psd} = \arg \max_c \cos(\hat{f}_j^t, p_c) \quad (8)$$

$$\sigma_i = \max_c \cos(\hat{f}_j^t, p_c) \quad (9)$$

where σ_i serves as the confidence score for the assigned pseudo-label y_i^{psd} .

Adaptive Thresholding: Instead of using a fixed confidence threshold, we employ a curriculum learning strategy with increasing confidence ratio $\eta(t)$:

$$\eta(t) = \eta(0) + \frac{t}{T_{total}} \cdot (\eta_{max} - \eta(0)) \quad (10)$$

This progressive inclusion strategy strikes a balance between exploration (utilizing more target data) and exploitation (maintaining pseudo-label quality).

Confidence-based Partitioning: At each training step, target features are separated into two parts:

- Confident subset: $\hat{F}_t^{con} = \{(\hat{f}_i^t, y_i^{psd}) | \sigma_i \geq \eta(t)\}$;
- Distrusted subset: $\hat{F}_t^{dis} = \hat{F}_t \setminus \hat{F}_t^{con}$.

The dynamic partitioning serves two purposes: **(I)** Confident features directly participate in supervised aggregation with source data; **(II)** distrusted features undergo self-supervised consistency training, gradually improving their reliability to qualify for future supervised aggregation.

Hybrid Contrastive Optimization

At this stage, we perform operations on three distinct types of features: labeled source features \hat{F}_s , confident target features \hat{F}_t^{con} with reliable pseudo-labels, and distrusted target features \hat{F}_t^{dis} . The ultimate goal is to achieve effective category-wise aggregation, where same-category features are gathered and those from different classes are separated.

A straightforward approach would be to apply standard supervised contrastive learning to \hat{F}_s and \hat{F}_t^{con} while discarding distrusted \hat{F}_t^{dis} . Nevertheless, this strategy suffers from three fundamental limitations that compromise adaptation effectiveness. **(1) Underutilization of Target Data:** Discarding \hat{F}_t^{dis} represents a significant waste of target domain information, which could contribute to better representation learning; **(2) Emerging Distribution Divergence:** Focusing solely on confident target features creates a emerging distribution gap between the supervised subset $\{\hat{F}_s \cup \hat{F}_t^{con}\}$ and the excluded \hat{F}_t^{dis} , potentially undermining the domain-invariant property established by the Adv-LCIB module; **(3) Conflicting Optimization Objectives:** Without proper coordination, contradictory optimization pressures may arise between the discriminative clustering objective and the robust consistency objective.

To address above issues, we propose a hybrid contrastive optimization strategy that simultaneously leverages all three feature types through complementary loss functions. Instead of confining all features into a single optimization framework, we design specialized objectives that exploit the unique characteristics of each feature type while ensuring overall coherence. The supervised aggregation loss \mathcal{L}_{sup} as dominant constraint handles the reliable features to form robust discriminative clusters; the self-supervised consistency loss \mathcal{L}_{self} gradually enhances the confidence of distrusted target features; and the anti-divergence regularization \mathcal{L}_{anti} bridges the distribution gap between these two pathways.

Supervised Aggregation \mathcal{L}_{sup} : To enable direct semantic category-wise aggregation between source features and confident target features, DARSD treats \hat{F}_s and \hat{F}_t^{con} equally and conducts supervised contrastive learning on them using reliable labels. Specifically, for any feature $\hat{f}_i \in \{\hat{F}_s \cup \hat{F}_t^{con}\}$, we define the positive set $\mathcal{P}(i)$ as features sharing the same class label and its negative set $\mathcal{N}(i)$ as features from different classes. The supervised loss is formulated as:

$$\mathcal{L}_{sup} = \mathbb{E}_{\hat{f}_i \in \{\hat{F}_s \cup \hat{F}_t^{con}\}} \left[\mathbb{E}_{\hat{f}_p \in \mathcal{P}(i)} - \log \frac{\exp(\cos(\hat{f}_i, \hat{f}_p) / \tau)}{\sum_{\hat{f}_n \in \mathcal{N}(i)} \exp(\cos(\hat{f}_i, \hat{f}_n) / \tau)} \right] \quad (11)$$

where τ is the temperature parameter.

Self-supervised Consistency \mathcal{L}_{self} : For the distrusted target features, we employ self-supervised consistency learning to enhance their confidence rather than immediately introducing noise into the supervised aggregation, making them candidates for promotion to the confident set in future iterations. Each distrusted feature \hat{f}_i^{dis} is paired with its augmented view \hat{f}_i^{dis+} to form positive pairs, while

other distrusted features serve as negatives. This consistency objective maintains representational stability for distrusted features while preventing overfitting to potentially noisy pseudo-labels.

$$\mathcal{L}_{self} = \mathbb{E}_{\hat{f}_i^{dis} \in \hat{F}_t^{dis}} \left[-\log \frac{\exp(\cos(\hat{f}_i^{dis}, \hat{f}_i^{dis+})/\tau)}{\sum_{j \neq i} \exp(\cos(\hat{f}_i^{dis}, \hat{f}_j^{dis})/\tau)} \right] \quad (12)$$

Anti-divergence regularization \mathcal{L}_{anti} : A critical issue arises with the emerging distribution divergence caused by supervised aggregation and self-supervised consistency. Without proper coordination, these two optimization pathways may yield distinct feature distributions, violating the domain-invariant assumption and disrupting pseudo-label generation. Specifically, supervised aggregation produces cluster-wise distribution, while self-supervised consistency tends to generate uniform one (Cai et al. 2024b). To address this, we introduce an anti-divergence regularization that links distrusted target features to their semantically closest source counterparts. For each \hat{f}_i^{dis} , we identify its nearest semantic neighbor in the source domain by proximity searcher operator $PS(\cdot)$:

$$PS(\hat{f}_i^{dis}, \hat{F}_s) = \arg \max_{\hat{f}_j^s \in \hat{F}_s} \cos(\hat{f}_i^{dis}, \hat{f}_j^s) \quad (13)$$

The anti-divergence regularization loss then pulls each distrusted feature toward its identified source anchor, bridging mechanism prevents distribution heterogeneity of distrusted \hat{F}_t^{dis} and constrain distributional coherence across all feature types.

$$\mathcal{L}_{anti} = \mathbb{E}_{\hat{f}_i^{dis} \in \hat{F}_t^{dis}} \left[-\log \frac{\exp(\cos(\hat{f}_i^{dis}, PS(\hat{f}_i^{dis}, \hat{F}_s))/\tau)}{\sum_{\hat{f}_j^s \in \hat{F}_s} \exp(\cos(\hat{f}_i^{dis}, \hat{f}_j^s)/\tau)} \right] \quad (14)$$

Hybrid contrastive optimization creates a virtuous cycle where better clustering leads to more reliable prototypes, which in turn generate higher-quality pseudo-labels and expand the confident target pool. Meanwhile, improved consistency and distribution bridge provides more stable target features, promoting the conversion of distrusted target features into confident ones and reducing evolving distribution divergence. The final objective combines all these pathways with the adversarial loss from Adv-LCIB module:

$$\mathcal{L}_{total} = \mathcal{L}_{sup} + \mathcal{L}_{self} + \lambda_1 \mathcal{L}_{anti} + \lambda_2 \mathcal{L}_{adv} \quad (15)$$

where λ_1 and λ_2 are balancing hyperparameters.

Experimental Evaluation

Benchmarks and Evaluation Metrics

To demonstrate the effectiveness of our DARSD, we conduct comprehensive evaluations on four widely-used real-world benchmarks: **WISDM** (Kwapisz, Weiss, and Moore 2011), **HAR** (Anguita et al. 2013), **HHAR** (Stisen et al. 2015), and **MFD** (Lessmeier et al. 2016). These datasets represent diverse application domains. Detailed characteristics of each dataset are summarized in Table 1 and Appendix C.

Datasets	D	T	n_c	Subject	Train	Test
WISDM	3	128	6	30	1350	720
HAR	9	128	6	30	2300	990
HHAR	3	128	6	9	12716	5218
MFD	1	5120	3	4	7312	3604

Table 1: Characteristics of benchmarks.

We employ the **Macro-F1** score as primary evaluation metric for UDA tasks. This metric offers a comprehensive assessment of model performance by calculating the unweighted average of F1 scores across all classes, thus ensuring that both frequent and rare classes receive equal consideration in the evaluation process.

Baselines

We compare proposed DARSD framework against 12 state-of-the-art baselines. Based on their primary technical contributions, we categorize them into three distinct groups:

(1) Adversarial approaches: These methods leverage adversarial training mechanisms to align domain distributions, including VRADA (Purushotham et al. 2017), CDAN (Long et al. 2018), CoDATS (Wilson, Doppa, and Cook 2020), and CADT (Chen et al. 2024);

(2) Metric learning approaches: These techniques focus on learning domain-invariant representations through various distance metrics and alignment strategies, encompassing DDC (Tzeng et al. 2014), D-CORAL (Sun and Saenko 2016), CAN (Kang et al. 2019), HoMM (Chen et al. 2020), MMDA (Rahman et al. 2020), AdvSKM (Liu and Xue 2021), and DSAN (Zhu et al. 2021), and DARSD (ours);

(3) Self-supervised approaches: This category utilizes self-supervised learning paradigms for domain adaptation, represented by CLUDA (Ozyurt, Feuerriegel, and Zhang 2023).

Implementation Details

To ensure fair comparison across all methods, we adopt a consistent network architecture where the feature extractor is a Temporal Convolutional Network (TCN) with 4 layers, 128 hidden dimensions, 0.2 dropout ratio, and produces feature representations of length $d = 128$. The classification head consists of a two-layer MLP with 128 hidden dimensions and 0.1 dropout ratio. For our proposed DARSD framework, component-specific hyperparameters are configured as follows: In the Adv-LCIB module, the learnable basis $B_{obs}^{inv} \in \mathbb{R}^{d \times m}$ uses $m = 24$ basis vectors. The PPGCE component employs a confidence ratio η that starts at 0.1 and increases by 0.05 every 15 training batches. In hybrid loss function \mathcal{L}_{total} (Eq. (15)), anti-divergence loss \mathcal{L}_{anti} and adversarial loss \mathcal{L}_{adv} are balanced with equal weights of $\lambda_1 = \lambda_2 = 0.5$.

Performance Analysis

We compare DARSD with 12 UDA baselines on the WISDM, HAR, HHAR, and MFD benchmarks in Table 2.

DARSD achieves optimal performance in 35 out of 53 scenarios and ranks first across all datasets, demon-

Src → Trg	DDC	D-CORAL	VRADA	CDAN	CAN	CoDATS	HoMM	MMDA	AdvSKM	DSAN	CLUDA	CADT	DARSD
WISDM ; <i>Out of 19 scenarios, DARSD achieves the 15 optimal results and 3 runner-up positions.</i>													
0 → 13	0.319	0.608	0.441	0.381	0.319	0.347	0.577	0.288	0.563	0.577	0.409	<u>0.614</u>	0.625
1 → 24	<u>0.875</u>	0.746	0.750	0.360	0.515	0.500	0.418	0.360	0.304	0.676	0.812	0.381	1.000
2 → 28	0.669	0.726	0.688	0.644	0.610	0.688	0.691	0.677	0.742	0.654	<u>0.788</u>	0.693	0.822
4 → 11	0.309	0.585	0.264	0.231	0.146	0.226	0.207	0.226	0.211	0.578	<u>0.614</u>	0.448	0.712
5 → 12	0.484	0.511	0.573	0.094	0.521	0.473	0.508	0.086	0.515	0.405	0.518	0.653	<u>0.577</u>
7 → 2	0.496	0.490	0.399	0.543	0.490	0.494	0.494	0.459	0.476	0.481	0.576	<u>0.632</u>	0.667
7 → 26	0.412	0.396	0.308	0.344	0.395	0.405	0.406	0.385	0.416	0.401	0.403	<u>0.447</u>	0.456
Avg. Rank	7.21	6.84	7.00	9.89	8.26	8.16	6.79	11.2	7.26	8.58	4.11	<u>3.32</u>	1.42
HAR ; <i>Out of 11 scenarios, DARSD achieves the 6 optimal results and 4 runner-up positions.</i>													
2 → 11	0.372	0.670	0.680	0.358	0.644	0.434	0.545	0.374	0.385	0.428	0.644	0.782	<u>0.717</u>
3 → 20	0.671	0.853	0.847	0.549	0.769	0.852	0.828	0.757	0.860	0.784	0.968	0.864	<u>0.907</u>
5 → 18	0.552	0.595	0.715	0.491	0.636	0.626	<u>0.727</u>	0.462	0.668	0.663	0.659	0.710	0.745
7 → 13	0.511	0.436	0.680	0.442	0.530	0.505	0.611	0.388	0.533	0.639	<u>0.884</u>	0.886	0.681
9 → 18	0.453	0.665	<u>0.715</u>	0.357	0.362	0.389	0.508	0.319	0.461	0.590	0.610	0.653	0.846
12 → 16	0.446	0.663	<u>0.689</u>	0.655	0.500	0.432	0.678	0.385	0.446	0.561	0.582	0.585	0.832
13 → 19	0.774	0.716	<u>0.797</u>	0.548	0.619	0.852	0.852	0.582	0.828	0.906	0.811	0.864	
Avg. Rank	10.2	6.55	5.55	11.0	8.45	8.18	4.82	12.0	8.36	6.36	3.73	<u>3.64</u>	1.64
HHAR ; <i>Out of 13 scenarios, DARSD achieves the 9 optimal results and 4 runner-up positions.</i>													
0 → 2	0.605	0.569	0.536	0.611	0.598	0.598	0.627	0.612	0.628	0.415	0.710	0.585	<u>0.651</u>
0 → 4	0.266	0.261	0.284	0.264	0.257	0.253	0.317	0.214	0.341	0.443	<u>0.589</u>	0.410	0.619
1 → 6	0.678	0.725	0.702	0.727	0.621	0.696	0.726	0.693	0.662	0.696	<u>0.858</u>	0.782	0.861
2 → 3	0.297	0.437	0.380	0.338	0.408	0.444	0.303	0.253	0.393	0.598	0.582	<u>0.646</u>	0.692
2 → 4	0.231	0.305	0.415	0.431	0.294	0.320	0.230	0.192	0.219	0.143	0.526	0.464	<u>0.480</u>
4 → 0	0.175	0.249	0.243	0.273	0.165	0.222	0.179	0.162	0.163	0.116	<u>0.352</u>	0.304	0.483
4 → 1	0.456	0.461	0.545	0.667	0.523	0.469	0.607	0.517	0.466	0.488	<u>0.751</u>	0.646	0.796
Avg. Rank	9.38	7.31	6.85	6.77	7.54	9.00	6.62	10.7	9.15	9.00	<u>3.38</u>	3.85	1.31
MFD ; <i>Out of 10 scenarios, DARSD achieves the 5 optimal results and 2 runner-up positions.</i>													
0 → 3	0.531	0.513	0.463	0.598	0.468	0.614	0.504	<u>0.644</u>	0.493	0.439	0.605	0.546	0.716
1 → 3	0.940	0.892	0.521	0.987	0.625	0.994	0.940	0.997	0.930	<u>0.996</u>	0.900	0.765	0.997
2 → 1	0.893	0.714	0.493	0.997	0.587	<u>0.994</u>	0.849	0.971	0.887	0.993	0.559	0.613	0.953
0 → 2	0.762	0.490	0.494	0.772	0.477	0.502	0.540	0.701	0.508	0.426	0.689	0.555	<u>0.770</u>
3 → 2	0.737	0.695	0.485	<u>0.899</u>	0.564	0.906	0.729	0.783	0.728	0.846	0.790	0.686	0.813
2 → 0	0.659	0.609	0.445	<u>0.689</u>	0.489	0.669	0.613	0.594	0.562	0.627	0.628	0.637	0.792
3 → 0	0.573	0.527	0.474	0.552	0.471	0.679	0.521	0.526	0.507	0.511	0.626	<u>0.736</u>	0.756
Avg. Rank	5.70	8.90	12.4	<u>3.10</u>	10.8	<u>3.10</u>	7.80	4.80	9.10	8.50	7.50	6.90	2.10

Table 2: **Partial Macro-F1** results on WISDM, HAR, HHAR, and MFD benchmarks. Each result is the mean over ten random initializations. Src and Trg denote the source and target subsets. The best two results are highlighted by **1st** and 2nd. The remaining results appear in **Appendix Table 2**.

ing consistent superiority. On WISDM and HHAR, DARSD achieves an exceptional average rank of 1.42 and 1.31, substantially outperforming CADT (3.32) and CLUDA (3.38), respectively. This robust performance despite class imbalance demonstrates DARSD’s ability to effectively disentangle domain-invariant action modes information about from individual-specific artifacts. On MFD, a dataset fundamentally distinct from human activity benchmarks (*i.e.*, WISDM, HAR, and HHAR) due to its dense high-frequency and long-term industrial vibration signals, DARSD maintains competitive performance with an average rank of 2.10 compared to CDAN and CoDATS, both achieving an aver-

age rank of 3.10. This cross-scenario generalization from personal sensing to industrial monitoring validates the broad applicability of our explicit decomposition approach.

The comparative analysis illuminates advantages of our DARSD over existing paradigms. Adversarial methods (*e.g.*, CDAN and VRADA) exhibit inconsistent performance, as they risk eliminating not only domain-specific artifacts while also valid semantic information. Metric learning approaches (*e.g.*, HoMM and CADT) demonstrate moderate consistency. While the self-supervision method CLUDA performs strongly, relying on gradually and slowly contrastive learning and adversarial training. In contrast, our

ID.	Elements of DARSD					Src → Trg										
	LCIB	\mathcal{L}_{adv}	\mathcal{L}_{sup}	\mathcal{L}_{self}	\mathcal{L}_{anti}	WISDM 12 → 19	MF1	HAR 20 → 6	MF1	HHAR 8 → 6	MF1	WISDM 2 → 28	MF1	HHAR 7 → 4	MF1	Acc
1				✓	✓	0.435	0.727	0.667	0.694	0.052	0.183	0.450	0.711	0.055	0.199	
2	✓			✓	✓	0.795	0.838	0.866	0.878	0.808	0.803	0.800	0.804	0.749	0.756	
3	✓		✓	✓		0.606	0.818	0.808	0.823	0.783	0.777	0.713	0.770	0.708	0.725	
4	✓	✓	✓	✓		0.831	0.853	0.903	0.912	0.862	0.857	0.783	0.815	0.782	0.789	
5	✓	✓	✓	✓	✓	0.883	0.917	0.967	0.989	0.844	0.848	0.822	0.883	0.813	0.817	

Table 3: Ablation analysis of DARSD. Specifically, the contributions of LCIB, \mathcal{L}_{adv} , \mathcal{L}_{self} , and \mathcal{L}_{anti} are verified. The check mark (✓) denotes the activated components. We **bold** the best results and underline the runner-up positions.

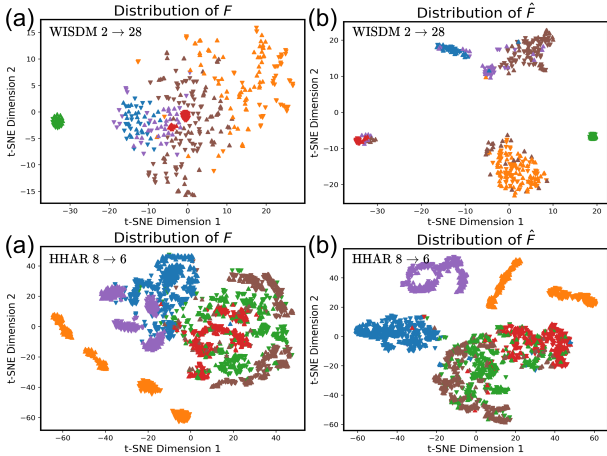


Figure 3: Distributions of F and \hat{F} . (a) and (b) illustrate distributions of F and corresponding \hat{F} , respectively. The **extensive examples** are displayed in **Appendix Fig. 1**.

DARSD framework provides more direct control over trade-off between invariance and discriminability, with faster convergence. The **Convergence Efficiency** of DARSD and CLUDA is compared in **Appendix D.4**. To better characterize performance of DARSD, we conduct **Representation Visualization** of source and target features in **Appendix D.3**.

Ablation Study

To validate the contribution of each component, we conduct comprehensive ablation studies across five randomly selected scenarios, progressively adding modules to demonstrate their individual and synergistic effects in Table 3.

Impact of Explicit Decomposition (LCIB): The comparison between ID.1 and ID.5 (full model) underscores the fundamental importance of explicit representation decomposition. Without LCIB module, performance degrades dramatically across all scenarios. This striking contrast validates the effectiveness of LCIB module in extracting semantic domain-invariant patterns. Consistent with Fig. 3, reconstructed domain-invariant features \hat{F} in Fig. 3b exhibit a more orderly distribution compared to those in Fig. 3a.

Necessity of Adversarial Training (\mathcal{L}_{adv}): Comparing ID.2 and ID.5 reveals that adversarial training is crucial

for ensuring the quality of B_{obs}^{inv} . Consistent improvements across all scenarios demonstrate that without adversarial constraints, LCIB may inadvertently capture domain-specific information, undermining the invariance property. This confirms the rationality of adversarial training of B_{obs}^{inv} .

Value of Target Feature Utilization (\mathcal{L}_{self} and \mathcal{L}_{anti}): The progression from ID.3 to ID.4 and then to ID.5 illustrates the importance of effective utilization of all \hat{F}_t . ID.3's performance shows that relying solely on \hat{F}_t^{con} leaves significant room for improvement. Incorporating self-supervised consistency (ID.4) yields notable gains, while anti-divergence regularization (ID.5) provides the final performance boost by bridging $\{\hat{F}_s \cup \hat{F}_t^{con}\}$ and \hat{F}_t^{dis} .

Synergistic Effects: The significant performance gap between any individual component and the full DARSD model demonstrates that its effectiveness arises from component synergy, not mere aggregation.

Notations: Due to space constraints, **A. Notation**, **B. Proof of Representation Space Decomposition**, **C. Detailed Benchmark Description**, **D.1. Macro-F1 Results**, **D.2. Hyperparameter Sensitivity Analysis**, **D.3. Representation Visualization**, **D.4. Convergence Efficiency**, and **E. Related Works** are provided in **Appendix**.

Conclusions

In this paper, we *for the first time* shift the paradigm of unsupervised time series domain adaptation from the perspective of explicit **representation space decomposition**. Building on this insight, we propose **DARSD**, disentangling domain-invariant patterns from domain-specific artifacts via a learnable invariant subspace basis. Additionally, DARSD decouples the optimization objectives of invariant feature extraction and robust cross-domain feature discriminative aggregation through Adv-LCIB and hybrid contrastive optimization with PPGCE modules. Extensive experiments conducted on **four benchmarks** demonstrate its superiority. Comprehensive studies prove the rationality of individual elements in DARSD and their synergy to achieve optimal performance. Future work will explore adaptive basis selection to further enhance the DARSD's applicability across diverse time series domains.

References

An, Y.; Zhang, K.; Chai, Y.; Li, Y.; and Zhu, Z. 2025. Feature Distillation-Based Uniformity Few-Shot Domain Adaptation for Cross-Domain Fault Diagnosis With Sample Shortage. *IEEE Transactions on Industrial Informatics*, 21(5): 3717–3726.

Anguita, D.; Ghio, A.; Oneto, L.; Parra, X.; and Reyes-Ortiz, J. L. 2013. A Public Domain Dataset for Human Activity Recognition using Smartphones. In *The European Symposium on Artificial Neural Networks*.

Cai, R.; Gao, W.; Peng, L.; Lu, Z.; Zhang, K.; and Liu, Y. 2024a. Debiased Contrastive Learning With Supervision Guidance for Industrial Fault Detection. *IEEE Transactions on Industrial Informatics*, 1–12.

Cai, R.; Peng, L.; Lu, Z.; Zhang, K.; and Liu, Y. 2024b. DCS: Debiased Contrastive Learning with Weak Supervision for Time Series Classification. In *ICASSP 2024 - 2024 IEEE International Conference on Acoustics, Speech and Signal Processing (ICASSP)*, 5625–5629.

Chen, C.; Fu, Z.; Chen, Z.; Jin, S.; Cheng, Z.; Jin, X.; and Hua, X.-S. 2020. Homm: Higher-order moment matching for unsupervised domain adaptation. In *Proceedings of the AAAI conference on artificial intelligence*, volume 34, 3422–3429.

Chen, Y.; Pan, Y.; Wang, Y.; Yao, T.; Tian, X.; and Mei, T. 2021. Transferrable contrastive learning for visual domain adaptation. In *Proceedings of the 29th ACM International Conference on Multimedia*, 3399–3408.

Chen, Y.; Yan, X.; Yang, Y.; Zhang, J.; Zhang, J.; Pan, L.; and Li, J. 2024. Disentangling domain and general representations for time series classification. In *Proceedings of the Thirty-Third International Joint Conference on Artificial Intelligence, IJCAI '24*. ISBN 978-1-956792-04-1.

Chuang, C.-Y.; Robinson, J.; Lin, Y.-C.; Torralba, A.; and Jegelka, S. 2020. Debiased contrastive learning. *Advances in Neural Information Processing Systems*, 33.

Cui, J.; Zhong, Z.; Tian, Z.; Liu, S.; Yu, B.; and Jia, J. 2023. Generalized Parametric Contrastive Learning. *IEEE Transactions on Pattern Analysis and Machine Intelligence*, 1–12.

Fang, Y.; Yap, P.-T.; Lin, W.; Zhu, H.; and Liu, M. 2024. Source-free unsupervised domain adaptation: A survey. *Neural Networks*, 174: 106230.

He, H.; Queen, O.; Koker, T.; Cuevas, C.; Tsiligkaridis, T.; and Zitnik, M. 2023. Domain adaptation for time series under feature and label shifts. In *Proceedings of the 40th International Conference on Machine Learning, ICML'23*. JMLR.org.

Huang, Y.; Peng, J.; Zhang, G.; Sun, W.; Chen, N.; and Du, Q. 2024. Adversarial Domain Adaptation Network With Calibrated Prototype and Dynamic Instance Convolution for Hyperspectral Image Classification. *IEEE Transactions on Geoscience and Remote Sensing*, 62: 1–13.

Jin, X.; Park, Y.; Maddix, D.; Wang, H.; and Wang, Y. 2022. Domain adaptation for time series forecasting via attention sharing. In *International Conference on Machine Learning*, 10280–10297. PMLR.

Kang, G.; Jiang, L.; Yang, Y.; and Hauptmann, A. G. 2019. Contrastive Adaptation Network for Unsupervised Domain Adaptation. In *Proceedings of the IEEE Conference on Computer Vision and Pattern Recognition*, 4893–4902.

Khosla, P.; Teterwak, P.; Wang, C.; Sarna, A.; Tian, Y.; Isola, P.; Maschinot, A.; Liu, C.; and Krishnan, D. 2020. Supervised contrastive learning. *Advances in neural information processing systems*, 33: 18661–18673.

Kwapisz, J. R.; Weiss, G. M.; and Moore, S. A. 2011. Activity recognition using cell phone accelerometers. *SIGKDD Explor. Newsl.*, 12(2): 74–82.

Lessmeier, C.; Kimotho, J. K.; Zimmer, D.; and Sextro, W. 2016. Condition monitoring of bearing damage in electromechanical drive systems by using motor current signals of electric motors: A benchmark data set for data-driven classification. In *PHM Society European Conference*, volume 3.

Litrico, M.; Del Bue, A.; and Morerio, P. 2023. Guiding Pseudo-labels with Uncertainty Estimation for Source-free Unsupervised Domain Adaptation. In *Proceedings of the IEEE/CVF Conference on Computer Vision and Pattern Recognition (CVPR)*.

Liu, Q.; and Xue, H. 2021. Adversarial Spectral Kernel Matching for Unsupervised Time Series Domain Adaptation. In *Proceedings of the Thirtieth International Joint Conference on Artificial Intelligence, IJCAI-21*, 2744–2750. International Joint Conferences on Artificial Intelligence Organization. Main Track.

Long, M.; Cao, Z.; Wang, J.; and Jordan, M. I. 2018. Conditional adversarial domain adaptation. In *Proceedings of the 32nd International Conference on Neural Information Processing Systems, NIPS'18*, 1647–1657. Red Hook, NY, USA: Curran Associates Inc.

Lu, J.; and Sun, S. 2024. CauDiTS: causal disentangled domain adaptation of multivariate time series. In *Proceedings of the 41st International Conference on Machine Learning, ICML'24*. JMLR.org.

Lu, N.; Xiao, H.; Ma, Z.; Yan, T.; and Han, M. 2024. Domain Adaptation With Self-Supervised Learning and Feature Clustering for Intelligent Fault Diagnosis. *IEEE Transactions on Neural Networks and Learning Systems*, 35(6): 7657–7670.

Ozyurt, Y.; Feuerriegel, S.; and Zhang, C. 2023. Contrastive Learning for Unsupervised Domain Adaptation of Time Series. In *The Eleventh International Conference on Learning Representations*.

Purushotham, S.; Carvalho, W.; Nilanon, T.; and Liu, Y. 2017. Variational Recurrent Adversarial Deep Domain Adaptation. In *International Conference on Learning Representations*.

Qu, S.; Zou, T.; He, L.; Röhrbein, F.; Knoll, A.; Chen, G.; and Jiang, C. 2024. LEAD: Learning Decomposition for Source-free Universal Domain Adaptation. In *Proceedings of the IEEE/CVF Conference on Computer Vision and Pattern Recognition (CVPR)*, 23334–23343.

Rahman, M. M.; Fookes, C.; Baktashmotlagh, M.; and Sridharan, S. 2020. *On Minimum Discrepancy Estimation for*

Deep Domain Adaptation, 81–94. Cham: Springer International Publishing. ISBN 978-3-030-30671-7.

Stisen, A.; Blunck, H.; Bhattacharya, S.; Prentow, T. S.; Kjærgaard, M. B.; Dey, A.; Sonne, T.; and Jensen, M. M. 2015. Smart devices are different: Assessing and mitigating mobile sensing heterogeneities for activity recognition. In *Proceedings of the 13th ACM conference on embedded networked sensor systems*, 127–140.

Sun, B.; and Saenko, K. 2016. Deep CORAL: Correlation Alignment for Deep Domain Adaptation. In *Computer Vision – ECCV 2016 Workshops*, 443–450. Cham: Springer International Publishing. ISBN 978-3-319-49409-8.

Tian, Y.; Krishnan, D.; and Isola, P. 2020. Contrastive Multiview Coding. In *Computer Vision – ECCV 2020*, 776–794. Cham: Springer International Publishing. ISBN 978-3-030-58621-8.

Tzeng, E.; Hoffman, J.; Saenko, K.; and Darrell, T. 2017. Adversarial discriminative domain adaptation. In *Proceedings of the IEEE conference on computer vision and pattern recognition*, 7167–7176.

Tzeng, E.; Hoffman, J.; Zhang, N.; Saenko, K.; and Darrell, T. 2014. Deep domain confusion: Maximizing for domain invariance. *arXiv preprint arXiv:1412.3474*.

Wang, P.; Yang, Y.; and Yu, Z. 2024. Multi-batch Nuclear-norm Adversarial Network for Unsupervised Domain Adaptation. In *2024 IEEE International Conference on Multimedia and Expo (ICME)*, 1–6.

Wang, T.; and Isola, P. 2020. Understanding contrastive representation learning through alignment and uniformity on the hypersphere. In *Proceedings of the 37th International Conference on Machine Learning*, ICML’20. JMLR.org.

Westfertel, T.; Yeh, H.-W.; Zhang, D.; and Harada, T. 2024. Gradual Source Domain Expansion for Unsupervised Domain Adaptation. In *Proceedings of the IEEE/CVF Winter Conference on Applications of Computer Vision (WACV)*, 1946–1955.

Wilson, G.; Doppa, J. R.; and Cook, D. J. 2020. Multi-source deep domain adaptation with weak supervision for time-series sensor data. In *Proceedings of the 26th ACM SIGKDD international conference on knowledge discovery & data mining*, 1768–1778.

Xie, Y.; Jin, L.; Zhu, C.; Luo, W.; and Wang, Q. 2025. Enhanced cross-domain lithology classification in imbalanced datasets using an unsupervised domain Adversarial Network. *Engineering Applications of Artificial Intelligence*, 139: 109668.

Xu, C.; Song, Y.; Zheng, Q.; Wang, Q.; and Heng, P.-A. 2025. Unsupervised multi-source domain adaptation via contrastive learning for EEG classification. *Expert Systems with Applications*, 261: 125452.

Yang, Y.; Zhang, C.; Zhou, T.; Wen, Q.; and Sun, L. 2023. Dcdetector: Dual attention contrastive representation learning for time series anomaly detection. In *Proceedings of the 29th ACM SIGKDD Conference on Knowledge Discovery and Data Mining*, 3033–3045.

Ye, X.; and Wang, K. I.-K. 2024. Deep generative domain adaptation with temporal relation attention mechanism for cross-user activity recognition. *Pattern Recognition*, 156: 110811.

Zha, H.; Shu, X.; Liu, C.; Zhang, Z.; Chen, J.; and Lin, Y. 2025. Cross-Domain Generalization for Specific Emitter Identification With Unseen Signals via Fourier Phase and MMD Features. *IEEE Internet of Things Journal*, 12(14): 28032–28042.

Zhang, H.; Zhang, Y.-F.; Zhang, Z.; Wen, Q.; and Wang, L. 2024a. LogoRA: Local-Global Representation Alignment for Robust Time Series Classification. *IEEE Transactions on Knowledge and Data Engineering*, 36(12): 8718–8729.

Zhang, K.; Cai, R.; Zhou, C.; and Liu, Y. 2024b. Debaised Contrastive Learning for Time-Series Representation Learning and Fault Detection. *IEEE Transactions on Industrial Informatics*, 20(5): 7641–7653.

Zhang, K.; Wen, Q.; Zhang, C.; Cai, R.; Jin, M.; Liu, Y.; Zhang, J. Y.; Liang, Y.; Pang, G.; Song, D.; and Pan, S. 2024c. Self-Supervised Learning for Time Series Analysis: Taxonomy, Progress, and Prospects. *IEEE Transactions on Pattern Analysis and Machine Intelligence*, 1–20.

Zhao, C.; Fang, G.; Ding, H.; Liu, X.; Wang, F.; Wang, G.; Zhao, K.; Wang, Z.; and Xi, W. 2025. Federated Multi-Source Domain Adaptation for mmWave-Based Human Activity Recognition. *IEEE Transactions on Mobile Computing*, 24(8): 7283–7296.

Zhao, J.; Deng, F.; He, H.; and Chen, J. 2021. Local Domain Adaptation for Cross-Domain Activity Recognition. *IEEE Transactions on Human-Machine Systems*, 51(1): 12–21.

Zhu, Y.; Zhuang, F.; Wang, J.; Ke, G.; Chen, J.; Bian, J.; Xiong, H.; and He, Q. 2021. Deep Subdomain Adaptation Network for Image Classification. *IEEE Transactions on Neural Networks and Learning Systems*, 32(4): 1713–1722.

Appendix

A. Notation

For easier reading, the crucial notations involved in this manuscript are summarized in Appendix Table 1.

Symbol	Formula	Definition
$x_i^s, x_j^t \in \mathbb{R}^{T \times D}$		Source and target samples
$\mathcal{S} = \{(x_i^s, y_i^s)\}_{i=1}^{n_s} \sim \mathcal{D}_s$		Source domain datasets following source distribution \mathcal{D}_s
$\mathcal{T} = \{x_i^t\}_{i=1}^{n_t} \sim \mathcal{D}_t$		Target domain datasets following target distribution \mathcal{D}_t
$B_{obs}^{inv} \in \mathbb{R}^{d \times m}$		Learnable common invariant basis
$w^{inv} \in \mathbb{R}^m$		Coordinate of feature in domain-invariant subspace
$\hat{w} \in \mathbb{R}^m$		Softmax regularized coordinate
$\hat{f}_i^s, \hat{f}_i^t \in \mathbb{R}^d$		Reconstructed domain-invariant features
$\hat{F}_s = \{\hat{f}_i^s\}_{i=1}^{n_s}$		Set of reconstructed source features
$\eta(t) \in [0, 1]$		Confidence ratio for \hat{F}_t
σ_i		Confidence score of \hat{f}_i^t
\hat{f}_i^{con}		Confident target feature
\hat{f}_i^{dis}		Distrusted target feature
$\hat{F}_t^{con} = \{\hat{f}_i^{con}\}_{i=1}^{\eta(t)n_t}$		Set of confident target features
$\hat{F}_t^{dis} = \{\hat{f}_i^{dis}\}_{i=1}^{(1-\eta(t))n_t}$		Set of distrusted target features
$\hat{F}_t = \{\hat{F}_t^{con} \cup \hat{F}_t^{dis}\}$		Set of reconstructed target features

Appendix Table 1: Specific description of crucial notations.

B. Proof of Representation Space Decomposition

B.1. Problem Setup

Consider a feature vector $f \in \mathbb{R}^d$ extracted from sample x . We decompose f into two orthogonal components:

$$f = f^{inv} + f^{spe} \quad (1)$$

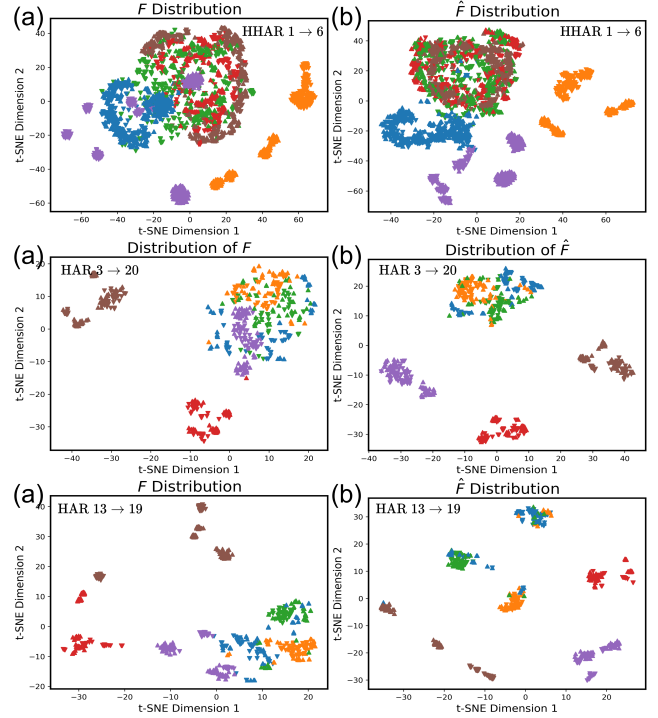
where f^{inv} and f^{spe} represent domain-invariant patterns and domain-specific noise, respectively.

B.2. Subspace Representation

We assume that \mathbb{R}^d can be decomposed into two orthogonal subspaces:

$$\mathbb{R}^d = \mathcal{S}^{inv} \oplus \mathcal{S}^{spe} \quad (2)$$

where \mathcal{S}^{inv} and \mathcal{S}^{spe} are the domain-invariant and domain-specific subspaces with dimensions m and $\bar{m} = d - m$, respectively.



Appendix Figure 1: **Extension of Figure 3 in main text.** Distributions of F and \hat{F} . (a) and (b) illustrate distributions of F and corresponding \hat{F} , respectively.

Let $B^{inv} \in \mathbb{R}^{d \times m}$ and $B^{spe} \in \mathbb{R}^{d \times \bar{m}}$ be orthonormal basis matrices for these subspaces such that:

$$\begin{aligned} (B^{inv})^\top B^{inv} &= \mathbf{I}_m, \\ (B^{spe})^\top B^{spe} &= \mathbf{I}_{\bar{m}}, \\ (B^{inv})^\top B^{spe} &= \mathbf{0}_{m \times \bar{m}} \end{aligned} \quad (3)$$

Then the decomposed components can be expressed as:

$$f^{inv} = B^{inv} w^{inv} \quad (6)$$

$$f^{spe} = B^{spe} w^{spe} \quad (7)$$

where $w^{inv} \in \mathbb{R}^m$ and $w^{spe} \in \mathbb{R}^{\bar{m}}$ are the coordinate vectors in their respective subspaces.

B.3. Domain-Invariant Component Extraction

Assumption: We have access to an observable approximation $B_{obs}^{inv} \in \mathbb{R}^{d \times m}$ of the true domain-invariant basis B^{inv} such that:

$$(B^{inv})^\top B_{obs}^{inv} = \mathbf{I}_m \quad (4)$$

This assumption implies that B_{obs}^{inv} spans the same subspace as B^{inv} and maintains orthogonality with B^{spe} .

Theorem: The domain-invariant coordinates can be extracted via projection:

$$w^{inv} = (B_{obs}^{inv})^\top f \quad (5)$$

Proof:

$$\begin{aligned} (B_{obs}^{inv})^\top f &= (B_{obs}^{inv})^\top (f^{inv} + f^{spe}) \\ &= (B_{obs}^{inv})^\top (B^{inv}w^{inv} + B^{spe}w^{spe}) \\ &= (B_{obs}^{inv})^\top B^{inv}w^{inv} + (B_{obs}^{inv})^\top B^{spe}w^{spe} \quad (6) \\ &= \mathbf{I}_m w^{inv} + \mathbf{0}_{m \times \bar{m}} w^{spe} \\ &= w^{inv} \end{aligned}$$

The key steps utilize:

1. Equation (4): $(B^{inv})^\top B^{inv} = \mathbf{I}_m$, which implies $(B_{obs}^{inv})^\top B^{inv} = \mathbf{I}_m$.
2. Orthogonality: $(B_{obs}^{inv})^\top B^{spe} = \mathbf{0}_{m \times \bar{m}}$.

B.4. Domain-Invariant Feature Reconstruction

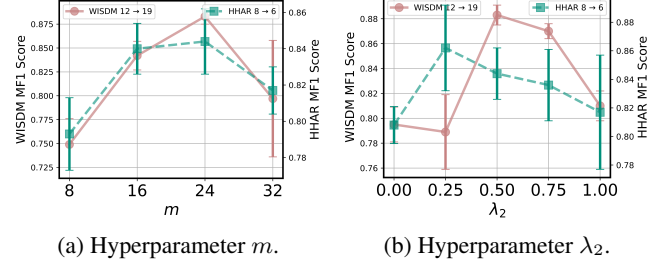
Once we obtain coordinate w^{inv} , we can reconstruct the domain-invariant component:

$$f^{inv} = B_{obs}^{inv} w^{inv} \quad (7)$$

C. Detailed Benchmark Description

The detailed backgrounds of WISDM, HAR, HHAR, and MFD benchmarks are displayed as follows:

- **Wireless Sensor Data Mining (WISDM) Dataset** (Kwapisz, Weiss, and Moore 2011): This dataset comprises 3-axis accelerometer measurements collected from 30 participants, sampled at a frequency of 20 Hz. Each measurement is segmented into non-overlapping segments of 128-time steps to predict the activity label for each participant. The dataset covers six activity labels: walking, jogging, sitting, standing, walking upstairs, and walking downstairs. Notably, the dataset poses challenges due to its imbalanced class distribution.
- **Human Activity Recognition (HAR) Dataset** (Anguita et al. 2013): This dataset features measurements from a 3-axis accelerometer, 3-axis gyroscope, and 3-axis body acceleration collected from 30 participants at a sampling rate of 50 Hz. The data is segmented into non-overlapping segments of 128-time steps for action classification. We classify the time series data into six types of activities: walking, walking upstairs, walking downstairs, sitting, standing, and lying down.
- **Heterogeneity Human Activity Recognition (HHAR) Dataset** (Stisen et al. 2015): This dataset comprises 3-axis accelerometer measurements from 30 participants, sampled at 50 Hz. Segmented into non-overlapping 128-time step sequences, the dataset aims to classify activities across six labels: biking, sitting, standing, walking, walking upstairs, and walking downstairs.
- **Machine Fault Diagnosis (MFD) Dataset** (Lessmeier et al. 2016): This dataset was collected by Paderborn University for bearing fault diagnosis, utilizing vibration signals to identify various types of incipient faults. The



Appendix Figure 2: Hyperparameter sensitivity analysis of m and λ_2 on WISDM 12 → 19 and HHAR 8 → 6 scenarios.

data were gathered under four distinct working conditions. Each sample consists of a single univariate channel containing 5,120 data points.

D. More Experimental Results

D.1. Macro-F1 Results

The Appendix Table 2 displays the remaining part of Table 2 in main text.

D.2. Hyperparameter Sensitivity Analysis

We analyze the sensitivity of two critical hyperparameters that govern our explicit decomposition approach: the dimensionality of the invariant basis m and the weight of adversarial training λ_2 .

Invariant Basis Dimensionality (m): Appendix Fig. 2a shows that optimal performance occurs at $m = 24$ for feature dimensions $d = 128$. This indicates that a 24-dimensional subspace provides sufficient capacity to capture essential semantic domain-invariant patterns, enabling effective domain adaptation. When $m < 24$, the invariant subspace B_{obs}^{inv} lacks sufficient capacity to capture semantic complexity, resulting in underfitting. When $m > 24$, the enlarged basis becomes harder to train effectively and more susceptible to incorporating domain-specific information, thereby undermining the invariance property.

Adversarial Training Weight (λ_2): Appendix Fig. 2b reveals stable performance within $\lambda_2 \in [0.25, 0.50]$, indicating robust optimization dynamics. When $\lambda_2 < 0.25$, insufficient adversarial pressure results in lossy reconstruction of domain-invariant information, causing significant information loss. When $\lambda_2 > 0.50$, excessive adversarial pressure forces the model to incorporate domain-specific information to maintain reconstruction consistency, compromising the invariance property.

Based on the sensitivity analysis, we recommend $m = 0.2d$ and $\lambda_2 = 0.5$ for general deployment. The consistent optimal ranges across different cross-domain scenarios demonstrate the robustness of DARSD’s explicit representation space decomposition approach.

D.3. Representation Visualization

Appendix Fig. 3 visualizes distributions of source and target features in the invariant subspace using t-SNE, provid-

Src → Trg	DDC	D-CORAL	VRADA	CDAN	CAN	CoDATS	HoMM	MMDA	AdvSKM	DSAN	CLUDA	CADT	DARSD
WISDM ; <i>Out of 19 scenarios, DARSD achieves the 15 optimal results and 3 runner-up positions.</i>													
10 → 14	0.541	0.337	0.591	0.266	<u>0.608</u>	0.477	0.667	0.469	0.471	0.337	0.510	0.599	0.691
10 → 21	0.694	0.250	0.125	0.118	0.250	0.390	0.313	0.390	0.694	0.106	0.250	<u>0.518</u>	0.392
12 → 7	0.632	0.486	0.437	0.546	0.636	0.612	0.442	0.539	0.655	0.574	<u>0.678</u>	0.620	0.834
12 → 19	0.396	0.317	0.410	0.298	0.508	0.456	0.281	0.233	0.510	0.518	<u>0.532</u>	0.518	0.883
15 → 29	0.299	0.265	0.391	0.238	0.372	0.136	0.208	0.133	0.299	0.182	<u>0.482</u>	0.441	0.529
18 → 20	0.383	0.379	0.578	0.600	0.389	0.427	0.421	0.280	0.348	0.268	0.673	<u>0.702</u>	0.658
19 → 2	0.459	0.501	<u>0.615</u>	0.312	0.327	0.403	0.522	0.306	0.460	0.428	0.458	0.555	0.664
21 → 16	0.537	0.669	<u>0.542</u>	0.404	0.641	0.410	0.669	0.310	0.523	0.568	0.595	0.850	0.787
25 → 22	0.273	0.241	<u>0.506</u>	0.401	0.241	0.200	0.307	0.159	0.309	0.341	0.375	0.500	0.610
26 → 2	0.414	0.618	0.517	0.404	0.362	0.598	0.519	0.453	0.463	0.424	<u>0.701</u>	0.610	0.731
28 → 2	0.484	0.495	0.473	0.400	0.412	0.492	0.511	0.430	0.484	0.451	0.710	0.606	<u>0.656</u>
28 → 20	0.571	0.620	0.672	0.605	0.655	0.578	0.699	0.537	0.557	0.615	0.703	<u>0.726</u>	0.728
Avg. Rank	7.21	6.84	7.00	9.89	8.26	8.16	6.79	11.2	7.26	8.58	4.11	<u>3.32</u>	1.42
HAR ; <i>Out of 11 scenarios, DARSD achieves the 6 optimal results and 4 runner-up positions.</i>													
18 → 21	0.439	0.760	0.697	0.450	0.449	0.857	0.803	0.380	0.439	0.588	0.920	<u>0.929</u>	0.948
20 → 6	0.643	0.776	0.619	0.407	0.593	0.659	0.935	0.407	0.586	0.588	<u>0.959</u>	0.782	0.967
23 → 13	0.398	0.586	0.683	0.298	0.509	0.439	0.539	0.518	0.401	0.723	<u>0.720</u>	<u>0.743</u>	0.764
24 → 12	0.724	0.765	0.658	0.758	0.872	0.709	0.893	0.448	0.736	0.826	0.866	0.768	<u>0.887</u>
Avg. Rank	10.2	6.55	5.55	11.0	8.45	8.18	4.82	12.0	8.36	6.36	3.73	<u>3.64</u>	1.64
HHAR ; <i>Out of 13 scenarios, DARSD achieves the 9 optimal results and 4 runner-up positions.</i>													
5 → 2	0.311	0.330	0.327	0.324	<u>0.338</u>	0.209	0.335	0.278	0.229	0.232	0.299	0.318	0.340
7 → 0	0.194	0.198	0.169	<u>0.454</u>	0.178	0.282	0.232	0.095	0.189	0.247	0.438	0.304	0.527
7 → 2	0.233	0.295	0.525	0.333	0.250	0.217	0.258	0.235	0.203	0.179	0.332	0.390	<u>0.392</u>
7 → 4	0.577	0.608	0.658	0.344	0.736	0.489	0.750	0.539	0.543	0.522	0.604	0.850	<u>0.813</u>
7 → 5	0.488	0.496	0.529	0.480	0.546	0.374	0.323	0.283	0.487	<u>0.649</u>	0.626	0.645	0.680
8 → 6	0.568	0.728	0.723	0.334	0.765	0.701	0.745	0.514	0.734	<u>0.467</u>	<u>0.837</u>	0.773	0.844
Avg. Rank	9.38	7.31	6.85	6.77	7.54	9.00	6.62	10.7	9.15	9.00	3.38	3.85	1.31
MFD ; <i>Out of 10 scenarios, DARSD achieves the 5 optimal results and 2 runner-up positions.</i>													
1 → 0	0.500	0.514	0.427	0.555	0.507	0.614	0.506	0.515	0.500	0.484	0.494	0.709	<u>0.663</u>
1 → 2	0.749	0.704	0.500	<u>0.881</u>	0.572	0.919	0.747	0.773	0.734	0.732	0.574	0.680	<u>0.776</u>
0 → 1	0.524	0.504	0.455	0.599	0.518	<u>0.607</u>	0.509	0.593	0.468	0.374	0.510	0.515	0.722
Avg. Rank	5.70	8.90	12.4	<u>3.10</u>	10.8	<u>3.10</u>	7.80	4.80	9.10	8.50	7.50	6.90	2.10

Appendix Table 2: **Extension of Table 2 in main text.** Macro-F1 results on WISDM, HAR, HHAR, and MFD benchmarks. Each result is the mean over ten random initializations. Src and Trg denote the source and target subsets. The best two results are highlighted by **1st** and 2nd.

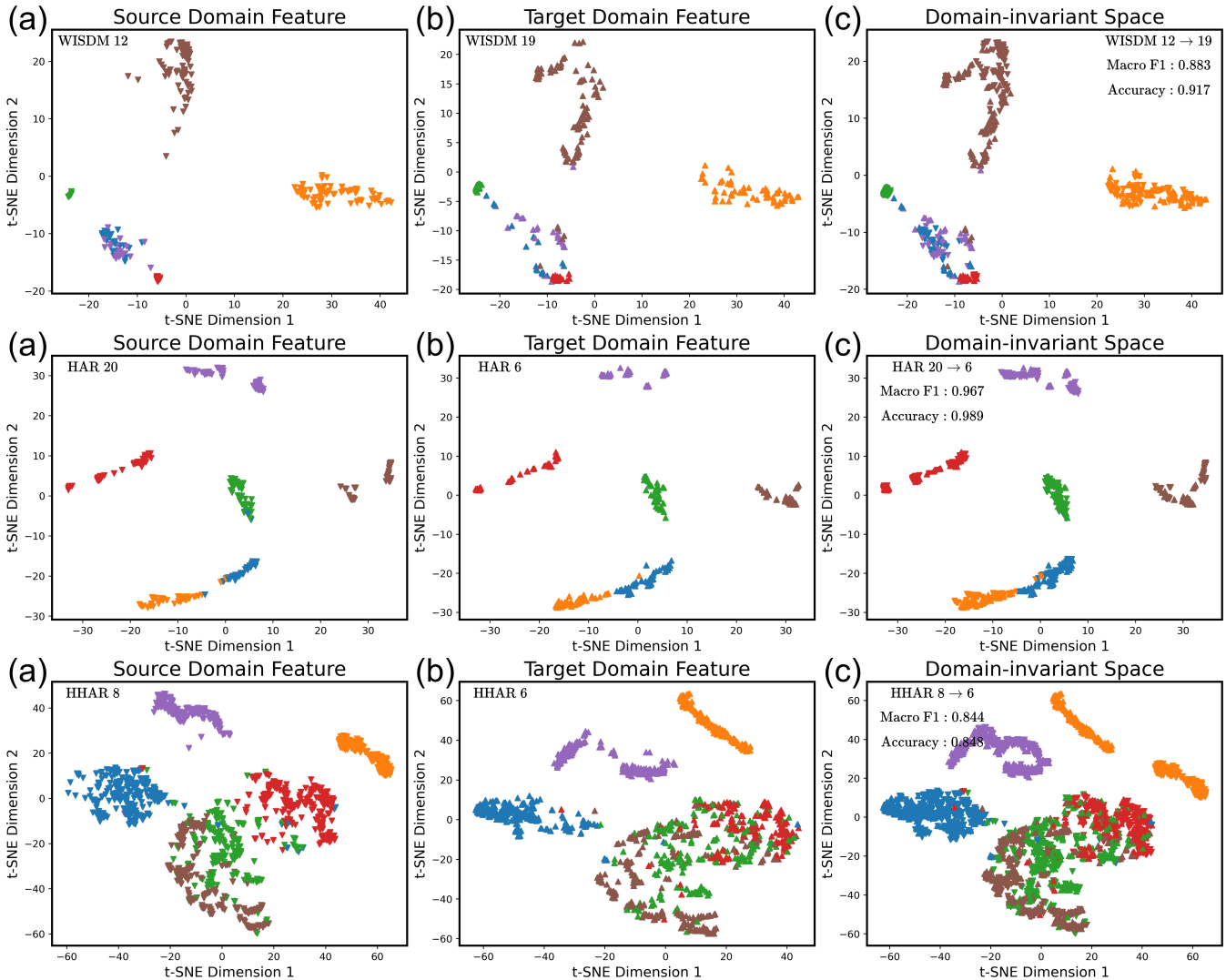
ing compelling evidence for DARSD’s effectiveness. Source features (Appendix Fig. 3a) form well-separated semantic clusters with distinct inter-class boundaries. Target features (Appendix Fig. 3b) display a remarkably similar geometric structure, where cluster shapes and relative positions mirror those of the source distribution. This structural preservation indicates that our Adv-LCIB module successfully extracts transferable domain-invariant semantic patterns while filtering domain-specific artifacts. Appendix Fig. 3c displays the substantial spatial overlap between source and target features of identical classes, alongside maintained inter-class separation. This confirms that our DARSD framework achieves dual objectives of domain invariance and semantic discriminability. Notably, explainable feature visualization validates that learned representations are truly domain-

agnostic, supporting our theoretical representation space decomposition framework and the effectiveness of PPGCE in the domain-invariant subspace.

D.4. Convergence Efficiency

Appendix Fig. 4 compares the convergence efficiency of DARSD and CLUDA across representative scenarios. DARSD consistently exhibits faster convergence, typically reaching stable performance within 50-80 epochs compared to CLUDA’s 100-150 epochs.

The efficiency advantage stems from separation strategies of optimization objectives of DARSD: the Adv-LCIB module explicitly constructs domain-invariant features, while hybrid contrastive optimization directly optimizes for discrimination in the invariant subspace. This reduces opti-



Appendix Figure 3: t-SNE visualization of DARSD feature distribution in the domain-invariant subspace. Colors distinguish different classes; downward (∇) and upward (Δ) triangles denote source and target features, respectively. Each row shows: (a) source features, (b) target features, and (c) combined source-target feature distribution in the domain-invariant subspace.

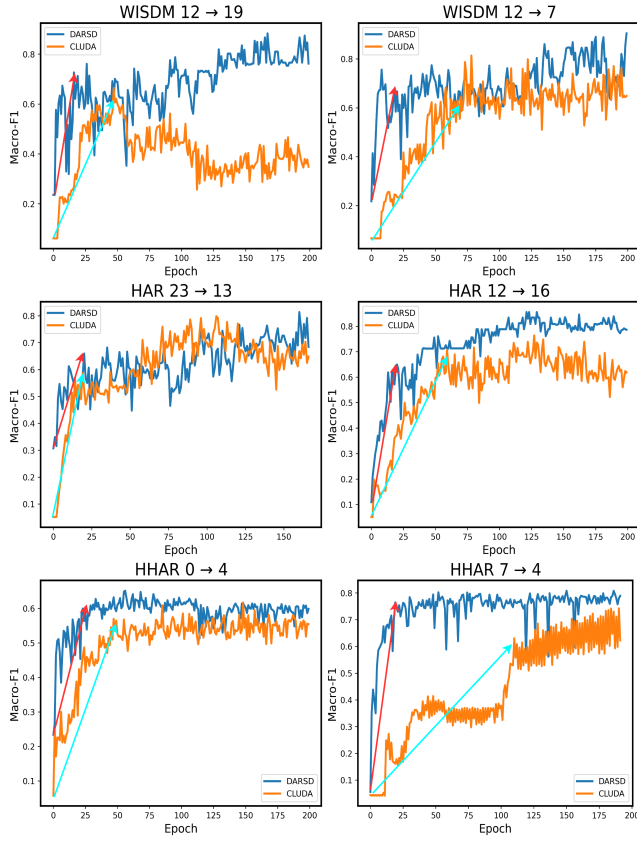
mization complexity compared to CLUDA, which simultaneously extracts domain-invariant representations and learns classification boundaries through a shared feature extractor, relying on indirect signals.

E. Related Works

E.1. Unsupervised Domain Adaptation

Unsupervised domain adaptation (UDA) seeks to transfer knowledge from an annotated source domain to an unlabeled target domain, where two domains have related yet different distributions. Despite significant progress, existing approaches suffer from a fundamental limitation: they treat representations as **monolithic entities** and strive to align **entire feature distributions**, failing to recognize that only part of components contain transferable knowledge.

They can be categorized into three groups: (1) **Adversarial Training Methods** represent the earliest paradigm for UDA (Tzeng et al. 2017), employing domain discriminators to learn domain-confusing representations. MBAN (Wang, Yang, and Yu 2024) and CPDIC (Huang et al. 2024) utilize adversarial training to align marginal distributions, while CoDATS (Wilson, Doppa, and Cook 2020) extends this framework to time series with multi-source adaptation. However, these methods suffer from a critical flaw: *the adversarial game fails to distinguish between transferable semantic content and domain-specific noise*, resulting in the elimination of essential information required for accurate classification. (2) **Metric Learning Approaches** aim to mitigate domain shift by explicitly minimizing statistical distances between domain distributions. Methods proposed in (Zha et al. 2025; Zhu et al. 2021) align second-



Appendix Figure 4: Comparisons of convergence efficiency of DARSD and CLUDA. The red and blue arrows indicate convergence trends of DARSD and CLUDA, respectively.

order statistics in Hilbert space, while other techniques like HoMM (Chen et al. 2020) perform high-order moment matching. Despite their theoretical grounding, these methods rely on an untenable assumption: that *entire feature vectors should be aligned*. This overlooks the compositional nature of representations, where only specific dimensions encode transferable knowledge. The introduction of domain-specific artifacts poisons the statistical properties of high-dimensional features, distorting their transferability across domains. **(3) Self-supervised Methods** leverage contrastive learning guided by pretext tasks to acquire domain-invariant representations. Approaches like CLUDA (Ozyurt, Feuerriegel, and Zhang 2023) progressively extract features via a MoCo architecture enhanced with adversarial training, while other studies (Xu et al. 2025; He et al. 2023; Jin et al. 2022) employ diverse pretext tasks to promote cross-domain consistency. Critically, *the design of pretext tasks directly governs the quality and transferability of the resulting domain-invariant information*.

Despite their methodological differences, all existing approaches share a common philosophical limitation: they rely on *implicit alignment mechanisms*. Whether via adversarial confusion, statistical distance minimization, or contrastive consistency, these methods presume that global fea-

ture alignment will simultaneously achieve domain invariance and preserve semantic content. This lack of explicit control over information preservation constitutes a critical weakness: *adaptation occurs without principled mechanisms to discern what knowledge is retained versus discarded during feature extraction*.

E.2. Contrastive Learning

Contrastive learning has emerged as a powerful representation learning paradigm that maximizes similarity between positive pairs while repulsing negative pairs (Tian, Krishnan, and Isola 2020; Yang et al. 2023; Zhang et al. 2024c). When applied to domain adaptation, however, it faces a fundamental challenge of defining meaningful cross-domain positive and negative pairs. **Sampling Bias** and **False Negatives** constitute a critical limitation in cross-domain contrastive learning. Standard approaches treat samples from different samples as negatives even when they belong to the same semantic class, introducing systematic bias that degrades representation quality (Wang and Isola 2020). Some methods attempt to address this through debiased sampling (Chuang et al. 2020) or supervised contrastive learning (Khosla et al. 2020). **Pseudo-labeling Strategies** have been proposed to enable supervised contrastive learning in domain adaptation scenarios (Cui et al. 2023; Litrico, Del Bue, and Morerio 2023). These approaches assign pseudo-labels to target features and use them to define positive/negative pairs. Given that classifier-predicted labels may be biased toward source domain characteristics, potentially causing error accumulation during training, pseudo-label derived from the statistical properties of target features distribution are more reliable.